Formatted: Width: 21 cm, Height: 29.7 cm

Reconstructing 3D subsurface salt flow

Stefan Back[1], Sebastian Amberg[1,2], Victoria Sachse[2,3], and Ralf Littke[2]

[1] Geological Institute, EMR, RWTH Aachen University, Germany
[2] Institute of Geology and Geochemistry of Petroleum and Coal, EMR, RWTH Aachen University, Germany
[3] Forschungszentrum Jülich GmbH, Projektträger Jülich, Germany

Correspondence to: Stefan Back (stefan.back@emr.rwth-aachen.de)

Abstract. Archimedes' principle states that the upward buoyant force exerted on a solid immersed in a fluid is equal to the weight of the fluid that the solid displaces. In this 3D salt-reconstruction study we treat Zechstein evaporites in the subsurface of the Netherlands, Central Europe, as a pseudo-fluid with a density of 2.2 g/cm^3, overlain by a lighter and solid overburden. 3D sequential removal (backstripping) of a differential sediment load above the Zechstein evaporites is used to incrementally restore the top Zechstein surface. Assumption of a constant subsurface evaporite volume enables the stepwise reconstruction of base Zechstein and the approximation of 3D salt-thickness change and lateral salt re-distribution over time.

The salt restoration presented is sensitive to any overburden thickness change irrespective if caused by tectonics, basin tilt, erosion or sedimentary process. Sequential analysis of lateral subsurface salt loss and gain through time based on Zechstein isopach difference maps provides new basin-scale insights into 3D subsurface salt flow and redistribution, supra-salt depocentre development, the rise and fall of salt structures, and external forces' impact on subsurface salt movement. The 3D reconstruction procedure described can serve as a template for analyzing other salt basins worldwide and provides a stepping stone to physically sound fluid-dynamic models of salt tectonic provinces.

1 Introduction

Archimedes (c. 246 BC) proposed - in short - that the upward buoyant force exerted on a solid body immersed in a fluid, whether fully or partially submerged, is equal to the weight of the fluid that the solid body displaces. This principle is an essential law of physics and fluid mechanics. In geoscience, it forms e.g. the foundation of Airy Isostasy (Airy, 1855). This study uses Archimedes' principle to reconstruct 3D subsurface salt flow through geological time by treating salt as a dense fluid phase (ρ = 2.2 g/cm^3) in which lighter overburden rocks (solids) float (Fig. 1a).

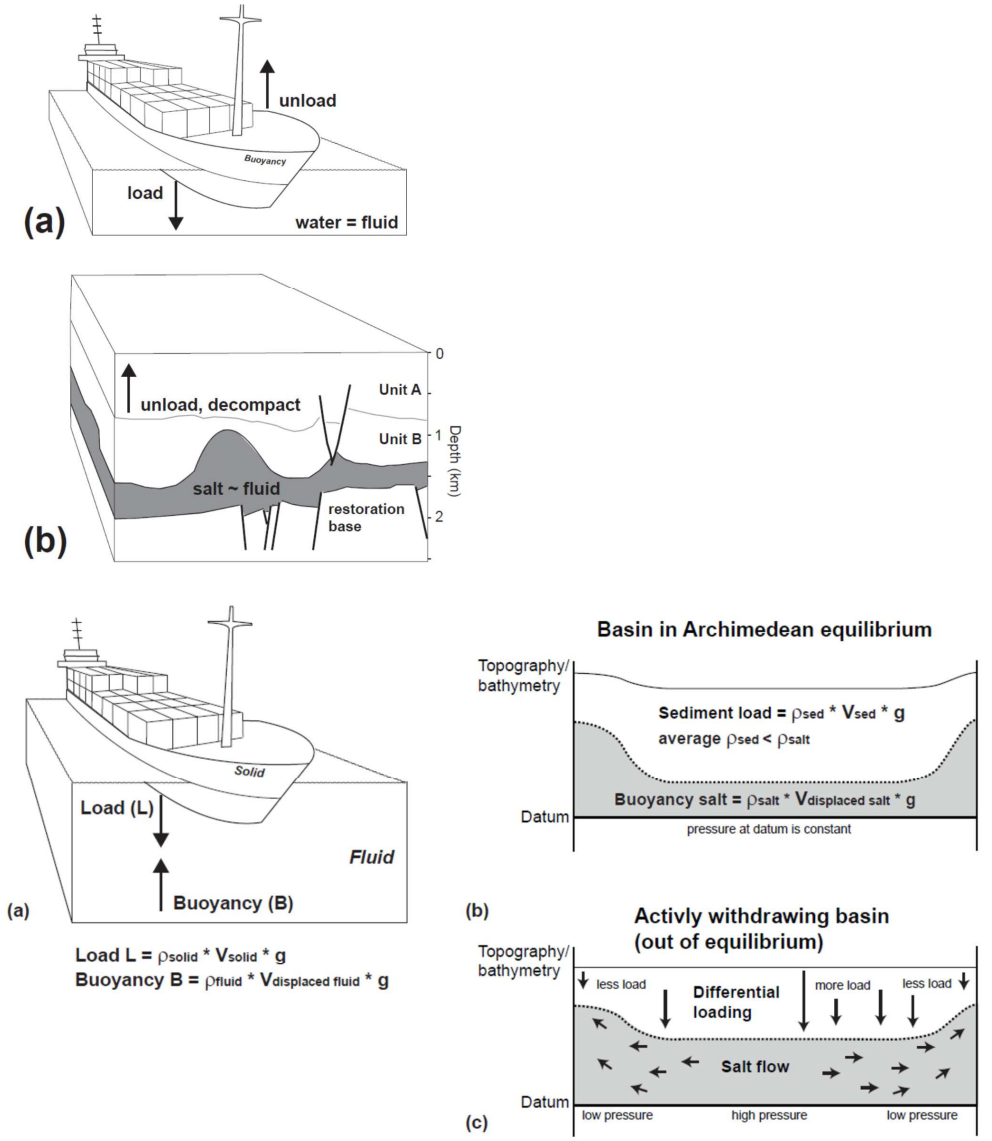

Figure 1. Archimedes' principle. (a) Ship loaded and unloaded floating on water. Buoyancy as upward force exerted by the fluid (water) that opposes the weight of the partially immersed ship. (b) Basin above subsurface evaporites in Achimedean equilibrium. Salt treated as dense pseudo-fluid (= 2.2 g/cm^3) loaded by cumulatively lighter overburden rocks (solid). Backstripping corresponds to incremental unloading of the overburden (sensu Maystrenko et al. 2013). Archimedean restoration of the Zechstein Basin example justified by slow subsurface salt flow. c) Basin out of equilibrium by major differential loading with significant salt flow and high differential pressure at datum level. ~~Cartoon of Archimedes' principle: (a) Ship loaded and unloaded floating on water. (b) Subsurface evaporites treated in analogy as dense pseudo-fluid (ρ = 2.2 g/cm3) loaded by overburden rocks (solid). Backstripping of this study corresponds to unloading of the overburden.~~

Formatted: Font: Not Bold
Formatted: Font: Not Bold
Formatted: Font: Not Bold
Formatted: Font: Not Bold, Superscript
Formatted: Font: Not Bold
Formatted: Font: Not Bold
Formatted: Font: Not Bold
Formatted: Font: Not Bold
Formatted: Font: Not Bold

The buoyancy driver for subsurface salt movement was already proposed over 100 years ago by Aarhenius and Lachmann (1912) and subsequently formalised by Barton (1933) and Nettleton (1934). Trusheim (1957, 1960) was a major proponent of this theory, and applied this approach of ~~analyzing~~ analysing salt flow to the NW European salt basin. In an early study on potential nuclear-waste storage sites, Kehle (1980) specified that "sediment loading, not buoyancy, sensu stricto", drives subsurface salt movement. Kehle (1988) pointed out several weaknesses in the original buoyancy theory mainly from a hydrodynamic perspective. He emphasized two main controls for salt flow, gravity head and pressure head, and stressed the importance of differential loading (resulting in high fluid-head gradients) for subsurface salt movement. Waltham (1997) quantitatively investigated non-buoyant causes of salt movement (compression causing overburden thickening; flexural overburden buckling; drag) and compared their effectiveness to buoyancy.

Few rocks behave as close as a Newtonian fluid as rock salt (e.g. Van Keken et al., 1993; Davison et al., 1996; Koyi, 2001; Gemmer et al., 2004; Hudec and Jackson, 2007; Jackson and Hudec, 2017). ~~Davison et al. (1996) estimated the ratio between sedimentary rock and evaporite rock viscosity ranging from 50 to 10000. Thus, salt, similar to any fluid, cannot support shear stress (Hudec and Jackson, 2007; Warren, 2016).~~ Various modelling studies have consequently treated subsurface salt as a pseudo-fluid flowing in the subsurface ~~and~~ considering its sedimentary overburden as solid (e.g. Jackson and Vendeville, 1994; Maystrenko et al., 2013). The assumption of the supra-salt stratigraphy floating on a thick subsurface salt layer requires salt, similar to a viscous fluid, to be in Archimedean (hydrostatic) equilibrium with the overburden (Fig. 1b). In such balance, the depletion of the subsurface salt layer will either be a passive response to differential loading by supra-salt sediments, or create ("actively", e.g. by dissolution) additional accommodation space to be loaded by sediment. In turn, thickening of the subsurface salt layer will either actively destroy supra-salt accommodation space or passively respond to an externally forced decrease of the salt overburden (e.g. localized erosion). ~~This~~ The Archimedean equilibrium approach with a solid overburden floating on an evaporite layer is supported by the observation that salt flows when loaded,~~;~~ and that faulting rather than folding ~~characterize~~characterises deformation in the overburden (Davison 2009; Warren, 2016). However, it must be recognized that all actively withdrawing basins are to some degree out-of-equilibrium (Fig. 1c). Yet, rather slow and local lateral salt flow, such as documented over large areas at various time intervals in this Zechstein Basin case study, can be seen as supporting a static Archimedean approach for salt reconstruction (Fig. 1b). The applicability of this method in salt provinces characterised by fast salt movement and the occurrence of large allochthonous salt bodies (e.g. Gulf of Mexico; Duffy et al., 2019) has yet to be studied.

~~In t~~In this 3D backstripping ~~study~~ exercise we ~~we avoid~~work around the complications of "fluid-dynamic" modelling of subsurface salt in that we simply measure 3D change in space through time (at Top salt) rather than simulating details of a salt-flow regime. ~~A governing assumption is that the studied overburden-salt system was in equilibrium throughout its history; i.e. that an isostatic relationship between the overburden and the salt substratum was maintained during crustal change induced~~

Formatted: Highlight
Formatted: Highlight
Formatted: Highlight
Formatted: Highlight
Formatted: Highlight
Formatted: Highlight
Formatted: Highlight
Formatted: Highlight
Formatted: Highlight

by tectonics, differential sedimentation and/or erosion. Elementary backstripping theory proved sufficient to determine areas of accommodation loss and gain through time by overburden restoration, no matter what the exact flow properties of salt or the cause for loss and gain of depositional space (e.g. tectonics, differential sedimentation, erosion). The backstripping and buoyancy compensation results presented are valid with the provision that salt flows into surplus space (salt gain), if available; and that subsurface evaporites will laterally move and redistribute when differentially loaded (salt loss); and that the subsurface salt volume remains constantand the state of stress exceeding the limiting yield point (Kehle 1988). The analysis of lateral subsurface salt loss and gain through time provides basin-scale insights into 3D subsurface salt movement, the development of supra-salt depocentres, the growth and decay of salt structures, and external forces' impact on salt systems. The 3D reconstruction procedure presented is mathematically easy and computationally quick. Various 1D, 2D, and 3D unloading and isostatic balancing algorithms that can be used to comprehendfor retracing the reconstruction presented approach are readily available in several several free and commercial geological interpretation and modelling software.

2 Study area, data and methods

The Late Permian Zechstein Group in the subsurface of the onshore Netherlands, Central Europe (Fig. 2a) comprises five evaporite cycles (Z1-Z5; Van Adrichem Boogaert and Kouwe, 1993; Geluk, 2007) with several hundreds of metres of rock salt and anhydrite deposited mainly in Z2 and Z3 (Fig. 2b). The Zechstein Group is overlain by the Lower and Upper Germanic Trias groups (RB, RN), the Early and Middle Jurassic Altena Group (AT), the Late Jurassic , Schieland (SL), Scruff (SG) and Niedersachsen (SK) groups (SL, SG, SK), the Early Cretaceous Rijnland Group (KN) and, the Late Cretaceous Chalk Group groups (CK), the Paleogene Lower (NL) and Middle (MN) North Sea groups and the Neogene to recent Upper North Sea Group (NU; Figs. 2b; 3a, b; TNO-NITG, 2004; Duin et al., 2006; Wong et al., 2007). For simplicity, this study treats the entire Permian Zechstein Group as one evaporite unit reacting to loading and unloading over geological time as a Newtonian fluid.

Seven 3D surfaces in depth (m) from the public 3D regional subsurface layer model of the Netherlands "DGM-deep v5" (TNO-NLOG, 2022) form the study's stratigraphic framework. Horizon and lithology data are from the NLOG and DINOLoket public databases. Fifteen individual 3D seismic-reflection volumes (in two-way-time (TWT); two volumes additionally pre-stack depth migrated) were used for the identification of key structural elements, subsurface salt occurrence, unconformities and overburden stratigraphy (Fig. 2). Conversion of subsurface data from time (ms TWT) to depth (m) and vice versa was based on the velocity model of Van Dalfsen et al. (2006).

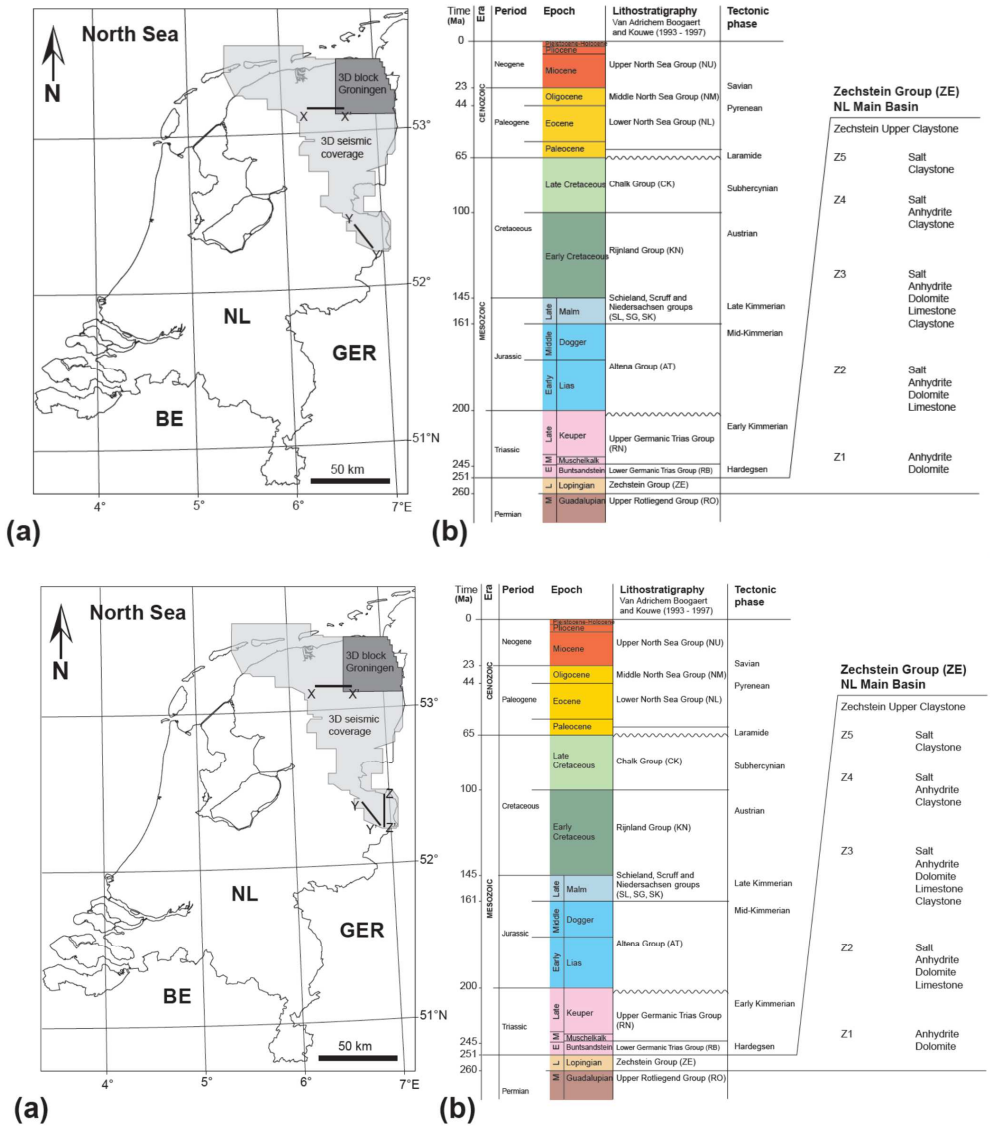

Figure 2. (a) Study area in the NE of the Netherlands and 3D seismic coverage. 3D block Groningen used for quality control. Lines X-X' and Y-Y' shown ~~on~~ in Figure 3. BE = Belgium; GER = Germany; NL = The Netherlands. (b) Stratigraphy of the study area (after Van Adrichem Boogaert and Kouwe, 1993). Detailed lithostratigraphic subdivision of the Zechstein Group on the right. Stratigraphic abbreviations used on following figures.

~~Seven 3D surfaces in depth (m) from the public 3D geological model of the Netherlands "DGM-deep v5" form the study's stratigraphic framework. Horizon and lithology data are from the NLOG and DINOLoket public databases. Fifteen~~

individual 3D seismic reflection volumes were used for the identification of key structural elements, subsurface salt occurrence, unconformities and overburden stratigraphy (Fig. 2). Conversion of subsurface data from time (ms TWT) to depth (m) and vice versa was based on the velocity model of Van Dalfsen et al. (2006).

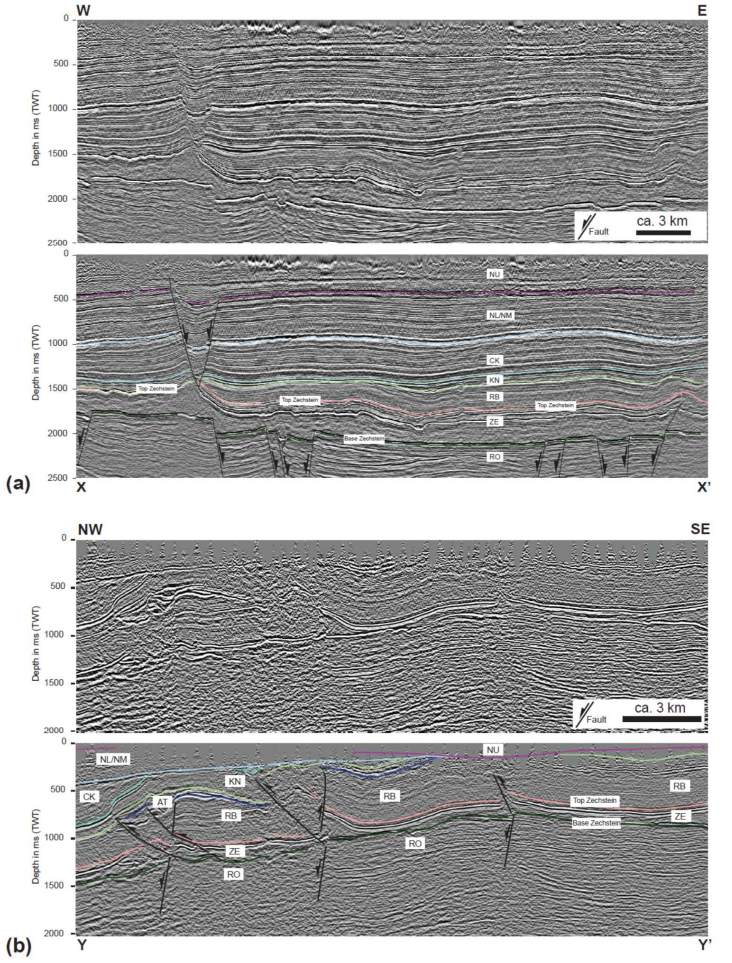
W
E
Depth in ms (TWT)
0
500
1000
1500
2000
2500
Fault
ca. 3 km
NU
NL/NM
CK
KN
RB
ZE
RO
Top Zechstein
Base Zechstein
(a)
X
X'
NW
SE
AT
(b)
Y
Y'

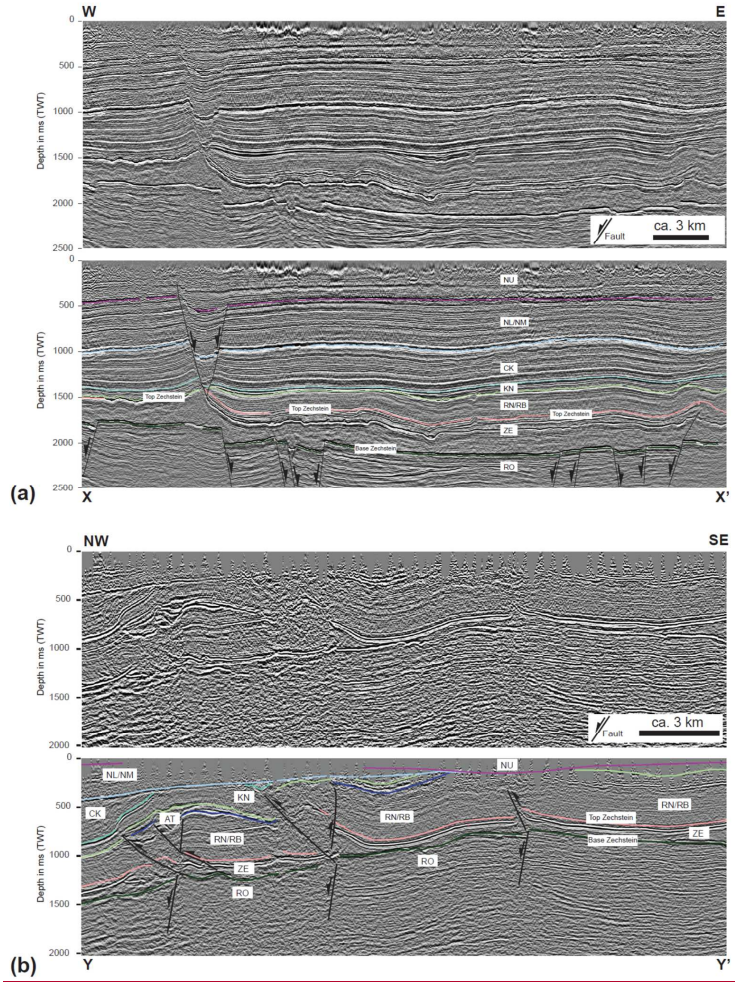

Figure 3. (a) Seismic-reflection line X-X' across the northern-central study area. Top – uninterpreted, base – interpreted. Note Zechstein unit (ZE) and bright, strong amplitude reflection near top imaging partly deformed and folded intra-salt Zechstein 3 stringer (Strozyk et al., 2012). (b) Seismic-reflection line Y-Y' across southern study area. Top – uninterpreted, base – interpreted. Note lack of upper Mesozoic and Cenozoic Zechstein overburden in the south. For line locations and stratigraphic abbreviations see Figure 2.

Backstripping for stratigraphic restoration and salt-flow monitoring was initially applied to individual 3D seismic-reflection volumes (a.o. ~~the~~ 3D block Groningen; Fig. 2a). The method proved simple, quick and effective and was therefore immediately extended to the entire (ca. 10,000 km^2) NE Netherlands. Strata above the Zechstein were assigned average lithologies (Table 1) with a compaction trend sensu Sclater and Christie (1980). In all cases the present-day cumulative average density of the column of vertical overburden (= grain density ~~and +~~ porosity; pores filled with water) was lighter than the ~~evaporate~~ evaporite substratum (fluid with $\rho = 2.2$ g/cm^3), and should have been so in the past.

Formatted: Indent: First line: 0 cm

Table 1: ~~Stratigraphy and average r~~Model rock properties based on stratigraphy and rock type (after Hunfeld et al. 2021) ~~used for backstripping and decompaction.~~; pores filled with water.

Lithostratigraphic Unit	Average Rock Type	Initial Porosity (%)	Depth Coefficient (km^{-1})	Grain density g/cm^3	Young Modulus (MPa)	Poisson Ratio
Upper North Sea Group	Sandstone	0.49	0.27	2.65	15000	0.29
Middle and Lower North Sea Group	Sandstone	0.49	0.27	2.65	15000	0.29
Chalk Group	Limestone	0.70	0.71	2.75	37500	0.32
Rijnland Group	ShalySand	0.56	0.39	2.68	23750	0.3
Schieland, Scruff and Niedersachsen Groups	ShalySand	0.56	0.39	2.68	23750	0.3
Altena Group	Shale	0.63	0.51	2.72	32500	0.3
Germanic Trias Group	Shale	0.63	0.51	2.72	32500	0.3
Zechstein Group	Shale	unbalanced	unbalanced	2.2	unbalanced	unbalanced

Formatted: Indent: First line: 0 cm

~~The~~ The reconstruction approach of this study differs from standard backstripping (e.g. Rowan, 2003; Maystrenko et al., 2013; Turcotte and Schubert, 2014) in that it does not apply any vertical shear restoration. After each unloading workstep a new model top surface was calculated by leaving the remaining overburden float on salt. As result there is a residual topography on each restored top surface. Figure 4 illustrates the general 3D reconstruction methodology applied, Figure 5 shows exemplarily a complete restoration sequence between the present-day and the Base Triassic (251 Ma) along 2D sections NORG XL8000 (line X-X') and TWENTE IL 9000 (line Z-Z').

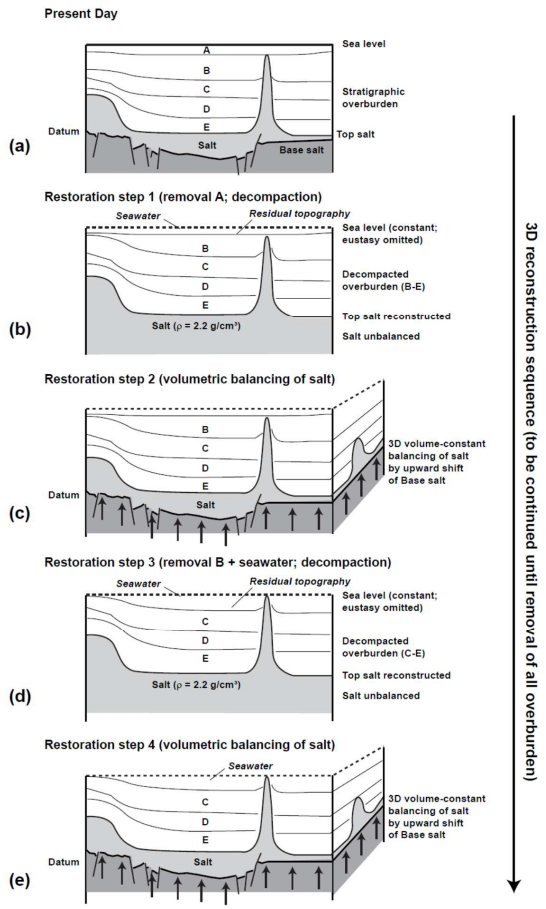

Figure 4. Restoration methodology. (a) Present-day situation. (b) Restoration step 1: Removal of top layer A. Airy-type vertical unloading of sedimentary column down to Top salt. Decompaction of sedimentary column down to Top salt (only restoration scenarios 2 and 3). Salt unit remains unbalanced. Residual topography flooded with seawater. (c) Restoration step 2: Upward vertical shift of unbalanced Base salt into new position constrained by keeping salt volume constant. (d) Same as restoration step 1 but removal of new top layer B. (e) Same as restoration step 2 with remaining stratigraphy. Entire 3D unloading procedure to be continued until removal of all salt overburden (Fig. 5).

The present-day structural framework formed the base for all restorations (Figs. 4-6). The first restoration step (e.g. Fig. 4a) removed the uppermost stratigraphic layer. As a result from unloading by stratal removal, the remaining stratigraphic column down to Top salt was readjusted by Airy-type vertical unloading (buoyancy compensation). Remnant space above the top pile of sediment up to sea level was then filled with seawater (e.g. Fig. 4b). Zechstein evaporites and any surface and unit below were excluded from unloading. Restoration step 2 then shifted the remaining, unbalanced Base Zechstein 3D surface vertically upward into a new position (e.g. Fig. 4c) constrained by keeping the subsurface Zechstein volume in the 3D framework model at its initial value (full study area ca. 6.38 x 10^{12} m^3). Zechstein thickness was then measured across the

Formatted: Indent: First line: 0 cm

Formatted: Highlight

study area and plotted as isopach map (Fig. 6). Unloading (restoration step 1), volumetric salt-balancing (restoration step 2) and salt-thickness measurement were recurrently repeated (see restoration steps 3 and 4; Figs. 4d and 4e) until the entire salt overburden was removed (e.g. Fig. 5).

The sensitivity of the 3D Zechstein-thickness reconstructions to varying backstripping parameters was tested using three different restoration scenarios. ~~Once a stratal cover unit was removed, the overburden response down to top Zechstein was to readjust due to buoyancy.~~ In restoration scenario 1, buoyancy compensation was local ("Airy isostasy" above salt), i.e. only vertically below the load~~., and Decompaction~~ decompaction was omitted from backstripping to produce the simplest reconstruction (Fig. 6a). In restoration scenario 2 (Figs. 5, 6b), buoyancy compensation was kept local ("Airy type") but decompaction of the overburden was included in backstripping. Restoration scenario 3 used flexural balancing instead of "Airy type" unloading in order to account for the cohesive strength of the overburden, and included decompaction (Fig. 6c). ~~Every~~ In scenario 3 every restoration step used the respective average overburden thickness calculated during the preceding workstep to define a new individual effective elastic thickness (Te) above salt. Irrespective of the scenario applied, after every unloading step the evaporite volume below the backstripped top Zechstein surface was readjusted and restored to the initial model volume (ca. 6.38 x 10^{12} m^3) by shifting the base Zechstein surface upwards. The geometry (external form) of the Zechstein base and the Zechstein volume were kept constant in all reconstruction steps.

~~salt. In all three scenarios the Zechstein evaporites and any surface and unit below were excluded from the unloading procedure.~~

~~**Table 1:** Stratigraphy and average rock properties (after Hunfeld et al. 2021) used for backstripping and decompaction.~~

~~Lithostratigraphic Unit~~	~~Average Rock Type~~	~~Initial Porosity (%)~~	~~Depth Coefficient (km^{-1})~~	~~Grain density g/cm^3~~	~~Young Modulus (MPa)~~	~~Poisson Ratio~~
~~Upper North Sea Group~~	~~Sandstone~~	~~0.49~~	~~0.27~~	~~2.65~~	~~15000~~	~~0.29~~
~~Middle and Lower North Sea Group~~	~~Sandstone~~	~~0.49~~	~~0.27~~	~~2.65~~	~~15000~~	~~0.29~~
~~Chalk Group~~	~~Limestone~~	~~0.70~~	~~0.71~~	~~2.75~~	~~37500~~	~~0.32~~
~~Rijnland Group~~	~~Shaly Sand~~	~~0.56~~	~~0.39~~	~~2.68~~	~~23750~~	~~0.3~~

Formatted: Highlight

Formatted: Indent: First line: 1.27 cm, Line spacing:

Formatted: Indent: First line: 1.27 cm

Formatted: Indent: First line: 1.27 cm, Line spacing:

Formatted: Indent: First line: 1.27 cm, Line spacing:

Formatted: Indent: First line: 1.27 cm, Line spacing:

Formatted: Indent: First line: 1.27 cm, Line spacing:

Formatted: Indent: First line: 1.27 cm, Line spacing:

Schieland, Scruff and Niedersachsen Groups	Shaly Sand	0.56	0.39	2.68	23750	0.3
Altena Group	Shale	0.63	0.51	2.72	32500	0.3
Germanic Trias Group	Shale	0.63	0.51	2.72	32500	0.3
Zechstein Group	Shale	unbalanced	unbalanced	2.2	unbalanced	unbalanced

Formatted: English (United States)
Formatted: Indent: First line: 1.27 cm, Line spacing:
Formatted: Indent: First line: 1.27 cm, Line spacing:
Formatted: Indent: First line: 1.27 cm, Line spacing:
Formatted: Indent: First line: 1.27 cm, Line spacing:
Formatted: English (United Kingdom)
Formatted: Indent: First line: 1.27 cm

After every unloading step, the evaporite volume below the backstripped top Zechstein surface was readjusted and restored to the initial model volume (ca. 6.38 x 10^{12} m^3) by shifting the base Zechstein surface upwards. The geometry (form) of the Zechstein base and the Zechstein volume were kept constant in all reconstruction steps. Unloading thus only caused surface change down to top Zechstein, which, when plotted against the (solely in height) adjusted but geometrically constant base Zechstein, enabled the calculation of a series of differential 3D salt thickness maps (Fig. 4). Resulting incremental changes in Zechstein thickness were then plotted as loss-gain (Fig. 5) and salt movement maps (Fig. 6).

Identical salt-thickness restoration results could have been achieved by moving the top Zechstein and overburden downwards to keep the salt volume constant. The This indicates that the restoration methodology proposed used is thus independent of a reference datum, but and consequently does not support referenced surface-topography analysis or palaeo-geographic reconstruction. The restoration approach in its current form is limited to incrementally backstrip the shallow post-salt overburden for the sole purpose of 3D true-to-volume reconstruction of the salt substratum, explicity excluding isostatic balancing of the isostatic crust-mantle relationshipequilibrium. The method therefore cannot be compared with classic crustal backstripping of salt systems (e.g. sensu Rowan, 2003; basic principles in Turcotte and Schubert, 2014).

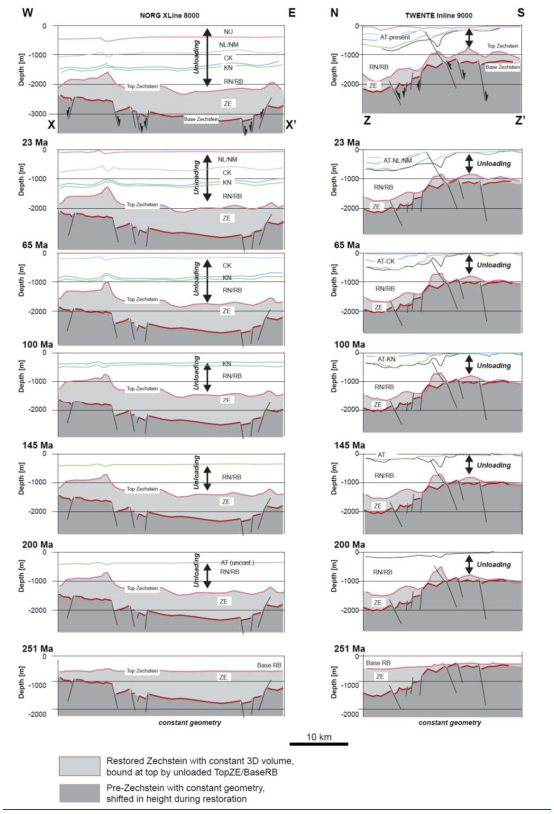

Figure 5. Restoration examples (scenario 2 - unloading and decompaction). Selected geological sections (X-X' = NORG XL 8000; Z-Z' = TWENTE IL 9000) through the 3D model that illustrate the sequential evolution of structure, stratigraphy and thickness of the Zechstein unit. Note absence of Jurassic strata (AT unconformity) along cross section X-X'. Also note pronounced flattening of Top salt towards 251 Ma. For illustration of 3D salt-thickness change and 3D subsurface salt flow through time see Figures 6 to 8. For location of sections see Figures 2 and 6-10).

3 Salt thickness reconstruction and salt loss-gain plots

True-to-volume Zechstein unloading in six time steps of ca. 25 - 50 Myrs duration restored the 3D subsurface evaporite thickness and distribution between today and 251 Ma (Fig. 46). Key differences between the three example scenarios are the omission (Fig. 4A6A) versus the inclusion of overburden decompaction during backstripping (Figs. 4b6b, c); and the use of pure vertical unloading ("Airy unloading"; Figs. 4a 6a and b) versus flexural overburden balancing (Fig. 4c6c). At first sight, Zechstein isopachs between today and 200 Ma appear in all reconstructions relatively similar. A significant difference

~~characterize~~characterises all three restoration scenarios in the interval between 200 and 251 Ma. At 251 Ma, all reconstructions restore major Zechstein thickness maxima (>1.5 km) in the Lower Saxony Basin (LSB) and in the northern Lauwerszee Trough (LT), irrespective of the reconstruction approach used (Fig. ~~4~~6). Few isolated thickness maxima remain more or less fixed at all times in restoration scenarios 1 and 2 that apply pure vertical unloading (Figs. ~~4a~~6a, b). These maxima correspond to piercement salt diapirs (e.g. Pieterburen, Winschoten) that remain unbalanced due to the lack of a vertical overburden. Such unbalanced salt structures account for less than 5% of the total Zechstein model volume in scenarios 1 and 2 (Figs. 6a, b). In restoration scenario 3, salt piercement structures change their shape during reconstruction due to overburden flexure affecting neighbouring areas.

In contrast to the rather subtle differences in Zechstein isopachs (Fig. 6), the difference plots between successive pairs of isopach maps (Figs. 7 and 8) show considerable variation. Salt loss and gain is local and represents lateral flow of salt within the model. Loss represents salt withdrawal and lateral expulsion; gain represents local salt inflation by salt influx. Salt loss and gain in the range of of several hundreds of metres to >1 km are highest in all restoration scenarios in the Triassic (251 - 200 Ma); at this time, major salt loss characterises the LSB, less salt loss the northern LT (Fig. 7). In all restoration scenarios salt escape is mainly to the Friesland Platform (FP) and Groningen High (GH), both gaining between ca. 500 m (Scenario 2, Fig. 7b) and 900 m (Scenario 3, Fig. 7c) of evaporites. The Jurassic (200-145 Ma) difference maps display uniform salt gain across most of the study area due to the presence of the Base Cretaceous unconformity. The LSB shows in this time subsurface salt loss between 150 m (Scenario 1, Fig. 7a) and 300 m (Scenario 3, Fig. 7c); the FP shows salt loss between 30 and 90 m (Fig. 7).

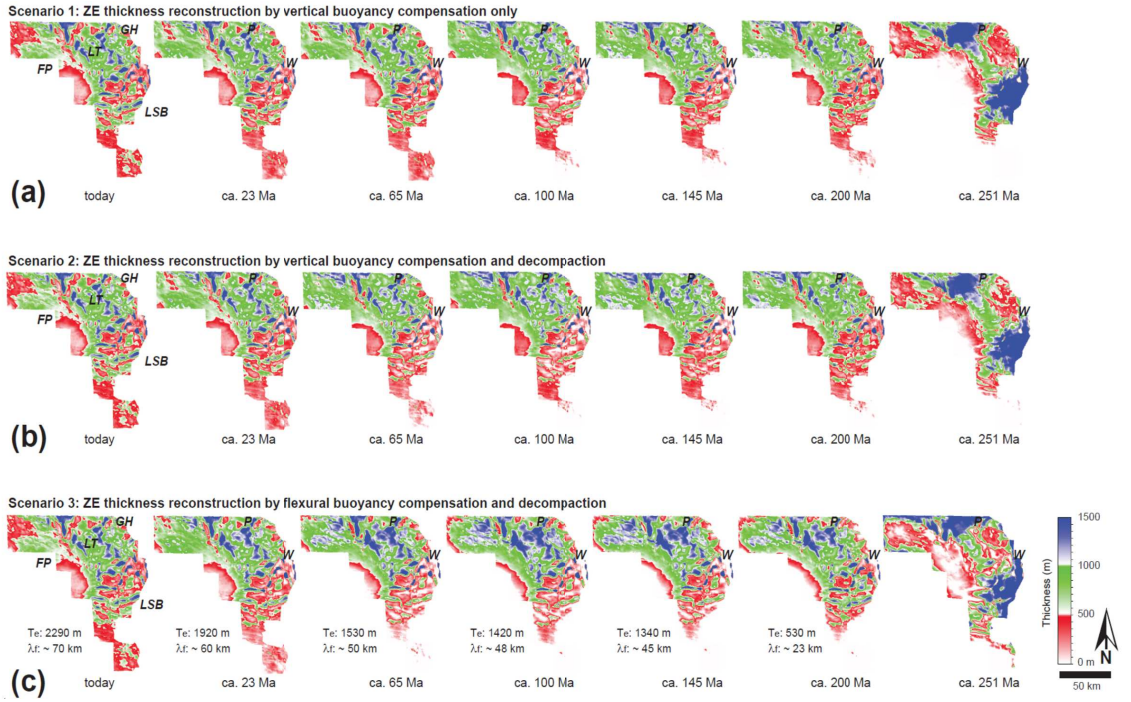

Figure 46. 3D Zechstein thickness-reconstruction results by backstripping. Note 251 Ma thickness maximum of Zechstein in Lower Saxony Basin (LSB) and Lauwerszee Trough (LT) in all reconstructions. (a) Backstripping scenario 1 – restored Zechstein thicknesses by vertical buoyancy compensation ("Airy balancing") omitting decompaction. (b) Backstripping scenario 2 - restored Zechstein thicknesses by vertical buoyancy compensation ("Airy balancing") including decompaction. (c) Backstripping scenario 3 - restored Zechstein thicknesses by flexural buoyancy compensation including decompaction. Effective elastic thickness (Te) of the overburden calculated as average overburden thickness from preceding restoration step; note corresponding change of flexural wavelength (f) during backstripping. All reconstructions using submarine conditions. FP = Friesland Platform; GH = Groningen High; P = Pieterburen; W = Winschoten. 2D restoration (scenario 2) extracted along sections X-X' and Z-Z' (see (a), 251 Ma) shown in Figure 5.~~3D Zechstein thickness-reconstruction results by backstripping. Note 251 Ma thickness maximum of Zechstein in Lower Saxony Basin (LSB) and Lauwerszee Trough (LT) in all reconstructions. (a) Backstripping scenario 1 – restored Zechstein thicknesses by vertical buoyancy compensation ("Airy balancing") omitting decompaction. (b) Backstripping~~

Formatted: English (United States)

Formatted: Justified

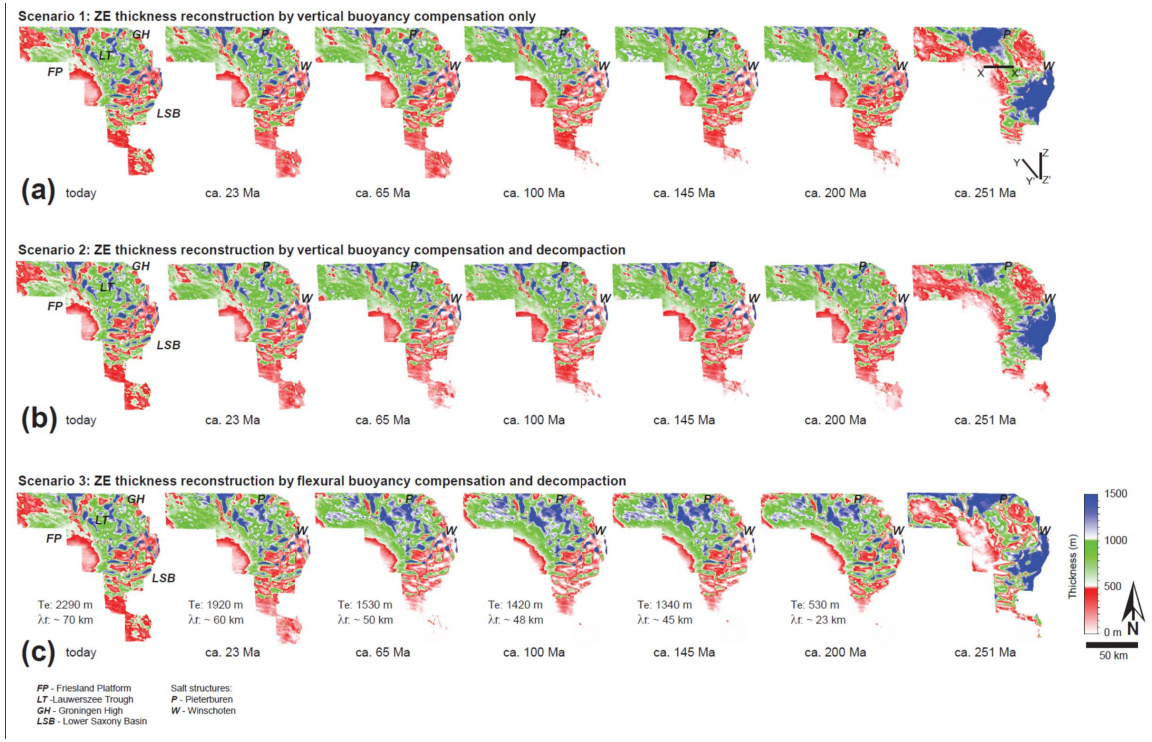
Scenario 1: ZE thickness reconstruction by vertical buoyancy compensation only
Scenario 2: ZE thickness reconstruction by vertical buoyancy compensation and decompaction
Scenario 3: ZE thickness reconstruction by flexural buoyancy compensation and decompaction
GH
LT
FP
LSB
P
W
(a) today
(b) today
(c) today
ca. 23 Ma
ca. 65 Ma
ca. 100 Ma
ca. 145 Ma
ca. 200 Ma
ca. 251 Ma
Te: 2290 m
λf: ~ 70 km
Te: 1920 m
λf: ~ 60 km
Te: 1530 m
λf: ~ 50 km
Te: 1420 m
λf: ~ 48 km
Te: 1340 m
λf: ~ 45 km
Te: 530 m
λf: ~ 23 km
Thickness (m)
1500
1000
500
0 m
N
50 km
FP - Friesland Platform
LT -Lauwerszee Trough
GH - Groningen High
LSB - Lower Saxony Basin
Salt structures:
P - Pieterburen
W - Winschoten

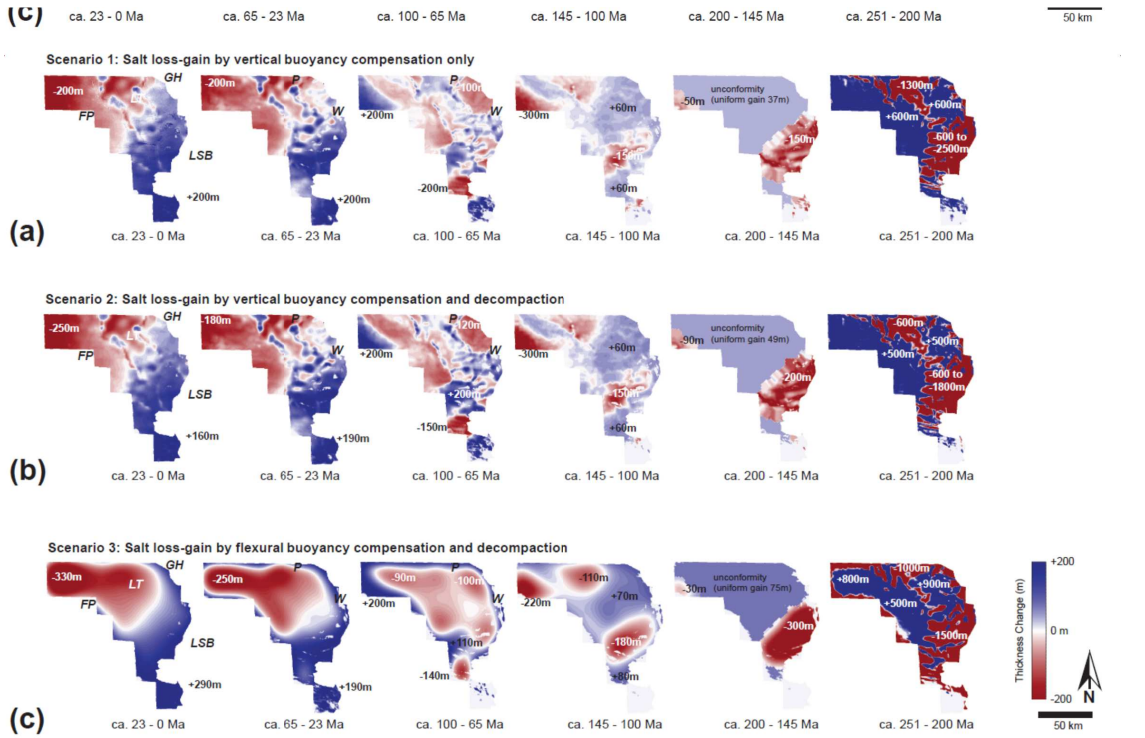

Figure 5~~7~~: Differences calculated between successive pairs of isopachs of Figure 6. (a) Salt loss-gain plot of backstripping scenario 1. (b) Salt loss-gain plot of backstripping scenario 2. (c) Salt loss-gain plot of backstripping scenario 3. Note similarity between vertical buoyancy compensation of backstripping scenarios 1 and 2 documenting limited significance of decompaction. Note pronounced difference between flexural buoyancy compensation (c) and vertical balancing (a, b) between recent time and the Early Cretaceous (145-100 Ma). Late Cretaceous salt gain pronounced in salt structures above LT boundary faults. 2D restoration (scenario 2) extracted along sections X-X' and Z-Z' (see (a), 251 Ma) shown in Figure 5.~~Differences calculated between successive pairs of isopachs of Figure 4. (a) Salt loss-gain plot of backstripping scenario 1. (b) Salt loss-gain plot of backstripping scenario 2. (c) Salt loss-gain plot of backstripping scenario 3. Note similarity between vertical buoyancy compensation of backstripping scenarios 1 and 2 documenting limited significance of decompaction. Note pronounced difference between flexural buoyancy compensation (c) and vertical balancing (a, b) between recent time and the Early Cretaceous (145-100 Ma).~~

Formatted: Justified

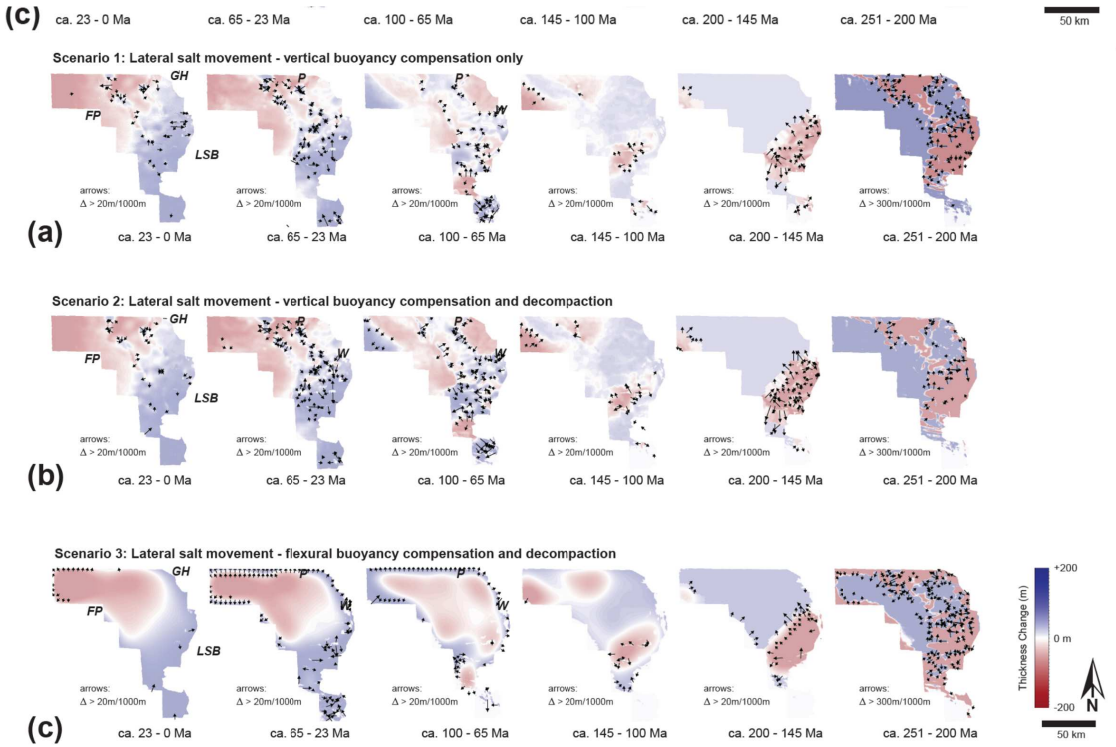

Figure 68: Maximum lateral change derived from difference plots of Figure 7. (a) Orientation of maximum lateral change based on backstripping scenario 1. (b) Orientation of maximum lateral change based on backstripping scenario. (c) Orientation of maximum lateral change based on backstripping scenario 3. Note pronounced edge effects at northern boundary of study area associated with flexural backstripping (scenario 3). 2D restoration (scenario 2) extracted along sections X-X' and Z-Z' (see a, 251 Ma) shown in Figure 5. 2D restoration (scenario 2) extracted along sections X-X' and Z-Z' (see (a), 251 Ma) shown in Figure 5.~~Maximum lateral change derived from difference plots of Figure 5. (a) Orientation of maximum lateral change based on backstripping scenario 1. (b) Orientation of maximum lateral change based on backstripping scenario. (c) Orientation of maximum lateral change based on backstripping scenario 3. Note pronounced edge effects at northern boundary of study area associated with flexural backstripping (scenario 3).~~

Formatted: Justified

~~structures account for less than 5% of the total Zechstein model volume in scenarios 1 and 2 (Figs. 4a, b). In restoration scenario 3, salt piercement structures change their shape during reconstruction due to overburden flexure affecting neighbouring areas.~~

~~In contrast to the rather subtle differences in Zechstein isopachs (Fig. 4), the difference plots between successive pairs of isopach maps (Figs. 5 and 6) show considerable variation. Salt loss and gain of several hundreds of metres to >1 km are highest in all restoration scenarios in the Triassic (251 – 200 Ma); at this time, major salt loss characterizes the LSB, less salt loss the northern LT (Fig. 5). In all restoration scenarios salt escape is mainly to the Friesland Platform (FP) and Groningen High (GH), both gaining between ca. 500 m (Scenario 2, Fig. 5b) and 900 m (Scenario 3, Fig. 5c) of evaporites. The Jurassic (200-145 Ma) difference maps display uniform salt gain across most of the study area due to the presence of the Base Cretaceous unconformity. The LSB shows in this time subsurface salt loss between 150 m (Scenario 1, Fig. 5a) and 300 m (Scenario 3, Fig. 5c); the FP shows salt loss between 30 and 90 m (Fig. 5).~~

Formatted: Highlight

The Early Cretaceous (145-100 Ma) shows in all restorations only minor changes in subsurface Zechstein distribution (Figs. ~~5~~7, ~~6~~8). Main salt-loss areas are the northern LSB and the eastern FP (Fig. ~~6~~8). Salt gain is mainly observed in the central and southern LT and along the Hantum fault zone (Fig. ~~7~~9). The Early Cretaceous (145-100 Ma; Fig. ~~5c~~7c) highlights the difference between flexural backstripping and vertical overburden balancing (Figs. ~~5a~~7a, b) in producing a smoothed, partially amplified salt loss and gain plot.

Between 100 and 65 Ma, the GH, LT and eastern FP comprised the main expulsion areas, whereas the LSB and FP locally received >200 m thickness of evaporites (Fig. ~~5~~7). Vertical balancing with and without decompaction (Figs. ~~5b~~7b, c) ~~documents~~ documented the growth of two narrow, parallel chains of NW-SE directed salt rollers, anticlines and walls above the main boundary faults of the LT (Fig. ~~7~~9). These structures received more salt between 65 and 23 Ma (Figs. ~~6a~~8a, b). The LSB accreted in the Paleogene and Neogene on average ca. 200 m of evaporites, respectively, likely sourced from the GH, LT, FP and from regions east (outside) of the study area (Figs. ~~5~~7, ~~6~~8). ~~Flexural~~ The flexural balancing approach (Figs. ~~5c~~7c, ~~6c~~8c) does not provide sufficient lateral resolution for the determination of Late Cretaceous to recent salt flow into individual salt structures.

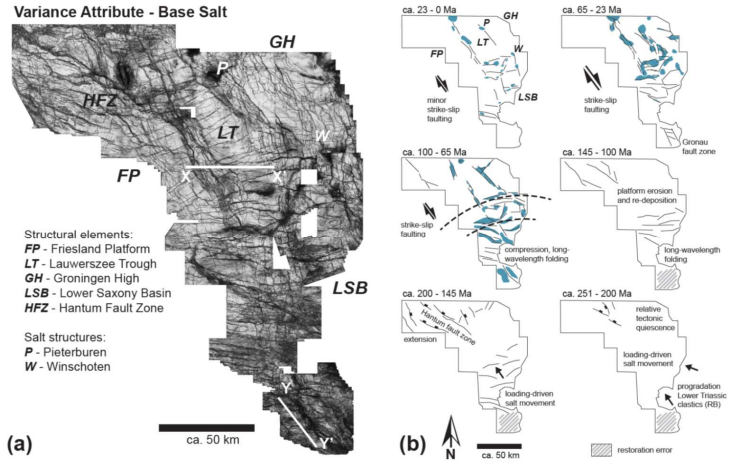

Figure ~~7~~9. (a) 3D variance horizon-slice highlighting main structures of the pre-Zechstein. Hantum Fault Zone (HFZ) between FP and LT ~~characterize~~characterised by significant salt gain in the Early Cretaceous. (b) Interpretation of relationship between sedimentary processes, tectonics and subsurface salt movement. ~~Lines~~ Seismic-reflection data along lines X-X' and Y-Y' shown on Figure 3. Blue colour indicating main salt structures.

4 Geological interpretation

The Zechstein isopach maps (Fig. 46), the evaporite loss-gain calculations (Fig. ~~5~~7), and the salt-movement plots (Fig. 68) provide important geological information when integrated with tectonic and seismic-stratigraphic analysis (Figs. 3a, b; 5, ~~7~~9; also see Cartwright et al., 2001; Giles and Rowan, 2012; Alsop et al., 2016; Khalifa and Back, 2021). Salt loss can be interpreted when ~~top~~ supra-salt strata forms a thickened overburden. If subsurface evaporites are completely expelled, a salt weld forms. Expulsion forces salt to move elsewhere, and salt either escapes to the surface and dissolves, or flows into salt structures overlain by an isopach thin, if rising syn-depositionally. Other isopach anomalies, e.g. elongate minima or maxima above basement-rooted structures (Figs. 3a, b; ~~4~~6-8, ~~5, 7a~~) can indicate tectonically triggered subsurface salt loss or gain.

The Zechstein thickness reconstructions ~~of Figure 4~~ document that ~~that mostonly~~ small parts of the study area ~~were constantly underlain by Zechstein evaporites~~experienced complete salt withdrawal~~, Exceptions are~~including ~~i)~~ several a series of large, elongate, mainly E-W-oriented salt welds in the northern LSB (Fig. 8), and ~~ii)~~ parts of the very south of the study area with a ~~complete~~ lack of reconstructed Zechstein between 200 and 100 Ma (e.g. Figs. 47, 8). ~~The loss-gain plots~~The salt-thickness reconstruction of the south indicates significant salt expulsion and initial diapirism between 251 and 200 Ma; insignificant gain and loss until ~~100~~ 65 Ma; and finally ~~allochthonous~~ salt accretion since 65 Ma (Figs. ~~5~~7, 69). The pre-65 Ma interpretation of the south must be, however treated with caution. Lack of much of the Mesozoic overburden due to erosion (Figs. 3a, b; 5, 46; 7) results in incomplete Top-Zechstein backstripping. The restored Zechstein base therefore locally

Formatted: Highlight
Formatted: Highlight
Formatted: Highlight
Formatted: Highlight
Formatted: Highlight
Formatted: Highlight
Formatted: Highlight
Formatted: Highlight
Formatted: Highlight
Formatted: Highlight
Formatted: Highlight
Formatted: Highlight

intersects the Zechstein top during unloading, producing ~~significant~~ potential restoration errors (Fig. 7). The locally restored 251 Ma salt thickness of the south (up to 200m) is yet similar to the salt-thickness reconstruction by Ten Veen et al. (2012).

Evaporite-thickness change (Fig. ~~5~~7) divided by the duration of each restoration interval documents that between 200 Ma and present-day, long-term Zechstein thickness change was up to ca. 15 m/Myr. Though low in rate, this change is significant for interpretations on period or epoch scale (Fig. ~~5~~7). For example, the ca. 150 m growth of salt ridges above the eastern and western boundary faults of the LT in the Late Cretaceous can be interpreted as reflecting overburden thinning due to inversion tectonics responding to Africa-Iberia-Europe convergence (sensu Kley and Voigt, 2008). The "Airy-type" salt-movement plots between 100 and 23 Ma (Figs. ~~6a~~8a; b) all show significant salt flow above pre-existing, re-activated faults (boundary faults LT; Figs. 3a, b; ~~7b~~9b) into salt diapirs and walls. It must be noted in this context that this regional 3D Zechstein Basin study did not restore any sub-salt fault movement, which locally limits the accuracy of the thickness reconstruction. However, even if included ~~this~~ the post-Triassic evaporite re-distribution ~~is~~ will likely remain generally small when compared to the Zechstein isopach change between 251 and 200 Ma (Figs. ~~4~~6, ~~5~~7~~).~~, which ~~The Triassic Zechstein re-distribution~~ is locally >1500 m (Fig. ~~5~~7). Long-term evaporite loss (period scale) in the LSB and LT is at this time >30 m/Myr. The Triassic evaporite expulsion can be interpreted as dominantly driven by sedimentary loading from the southeast during the Buntsandstein (duration <10 Myrs; Figs. 2, 3, 5, ~~4~~6, ~~7B~~9B) in an overall tectonically quiet basin (Mohr et al., 2005; Geluk, 2007; Vackiner et al. 2013; Strozyk et al., 2014). Thus, loading-driven salt flow might attain on epoch scale long-term rates of >150 m/Myr (in line with Zirngast, 1996; Kukla et al., 2008), which is significantly above the tectonics-driven long-term rate of up to ca. 10 m/Myr in the Late Cretaceous (Fig. ~~5~~7).

Formatted: Highlight
Formatted: Highlight
Formatted: Highlight
Formatted: Highlight
Formatted: Highlight
Formatted: Highlight

5 Discussion

~~3D application of the >2000 year old principle of Archimedes (c. 246 BC) in t~~The Zechstein salt system of the NE Netherlands allows regional 3D thickness reconstruction of subsurface evaporites over time; 3D measurement of subsurface salt loss and gain over time; 3D salt-flow reconstruction over time; and the estimation of long-term salt-flow rates. The reconstruction of 3D subsurface salt movement is – although in this study solely dependent on the ~~unloading~~ restoration of differential overburden thicknesses – not restricted to monitoring sedimentary processes only. Any process that results in differential overburden thickness (including tectonics) will be also be balanced, as exemplarily shown for Late Cretaceous and Paleogene diapir growth likely triggered by inversion tectonics (Figs. ~~5~~7, ~~6~~8).

Zechstein-thickness restoration enables monitoring the growth and decay of salt structures and salt welds, results that can be immediately applied in e.g. petroleum systems models or for constraining physical fluid-dynamic models. It must be however noted that the studied Zechstein unit is in nature internally heterogeneous (Fig. 2b), with both vertical and lateral facies variations. More competent lithologies are interbedded with the mobile Zechstein halite units including anhydrite and carbonate stringers (see strong intra-Zechstein reflector, Fig. 3a). Lithological heterogeneity gives rise to rheological

heterogeneity, which may have an impact on the associated buoyancy. It must be therefore acknowledged that the assumption of all Zechstein units as a homogeneous fluid of constant density is a major simplification and thus a likely source of errors.

The Zechstein-thickness reconstructions presented ~~salt loss, gain and movement plots~~ (Figs. 5, ~~6~~8) indicate that likely much of the internal structural complexity of the evaporite successions~~s~~ (for examples see Richter-Bernburg, 1980; Strozyk et al., 2012, 2014; Biehl et al., 2014) can be explained by recurrent changes between salt loss, salt gain and evaporite-flow direction through time. Although post-Triassic Zechstein thickness change was generally low in rate, it could have well been responsible for the internal deformation of the Zechstein succession with its various salt layers and intercalated limestones and anhydrites. The slow and rather localized lateral salt flow documented in this Zechstein backstripping study can be seen as key supporting argument for reconstructing subsurface salt flow with a static Archimedean approach.

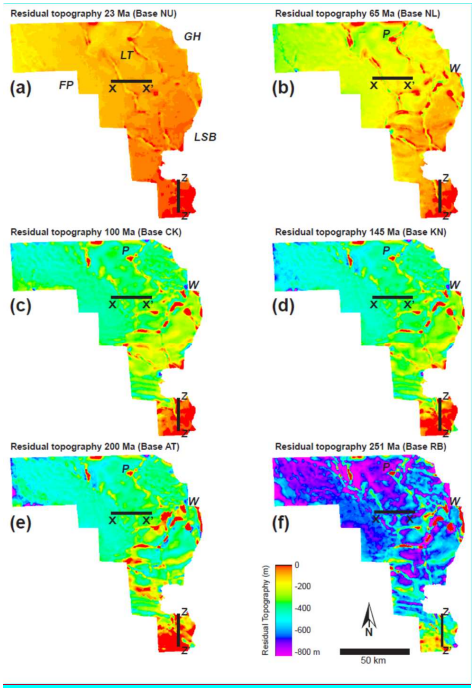

Figure 10. Residual 3D topography after each reconstruction step in scenario 2 (unloading and decompaction; submarine conditions). Depth position of respective model top at (a) 23Ma; (b) 65Ma; (c) 100Ma; (d) 145Ma; (e) 200Ma; and (f) 251 Ma. Note that residual topography does not represent palaeo-bathymetry. Incremental backstripping results in increasingly flat basin-floor topographies away from salt diapirs and ridges. Note piercement salt diapirs Pieterburen (P) and Winschoten (W) that remain unbalanced thoughout restoration. For balanced sections X-X' and Z-Z' see Figure 5.

~~Spatial evaporite redistribution through time seems both caused by but also causing highly variable intra-Zechstein stress conditions leading to complex polyphase and polydirectional 3D evaporite deformation (e.g. Fig. 3a).~~

Formatted: Highlight
Formatted: Highlight
Formatted: Highlight
Formatted: Highlight
Formatted: Indent: First line: 0 cm
Formatted: Indent: First line: 0 cm
Formatted: Highlight

Approximation of the top Zechstein as a horizontal surface at sea level after final unloading (situation at 251 Ma, all scenarios of Fig. ~~4~~6) can be potentially used to constrain~~s~~ the 251 Ma depth of the base Zechstein based on overburden unloading only. In other words, the assumption that the top Zechstein formed at base level roughly approximate~~s~~ the palaeo-depth location of the base Zechstein, determined from subtraction of the restored 251 Ma Zechstein thickness from the present-day sea level only. ~~It must be noted that t~~The validity of this approximation yet stands and falls with the validity of the zero-topography assumption for top Zechstein, as the Archimedean salt restoration ~~method~~ presented is not tied to any topographic reference level. Figure 10 shows the residual 3D topography after each reconstruction step of scenario 2 (i.e. unloading, decompaction, submarine conditions; see Figs. 5, 6b). The respective topography maps show an increasingly flat basin floor with a remnant topography confined to unbalanced salt diapirs and ridges. This configuration can be seen as another argument for the validity of the Archimedean restoration approach in the Zechstein study example. True palaeo-topographic referencing, potentially providing an alternative quality control for the differential salt thickness calculation, ~~could~~ however can only be achieved by integrating crustal isostatic balancing above the earth's mantle (Fig. 11; Rowan, 2003; Turcotte and Schubert, 2014) contemporaneously to salt-redistribution modelling into the restoration process. We have not yet found a technical solution for such an integration; crustal isostatic balancing remains therefore excluded from this balancing study.

Key limitations of the Zechstein reconstruction presented are the incomplete restoration due to overburden unconformities; omission of subsalt deformation from restoration; lack of knowledge on loss of salt at piercement structures; and potential loss or influx of salt at the edges of the study area. Incomplete salt restoration due to overburden erosion primarily affects the south (Figs. 5, ~~4~~6; ~~7b~~9b); incomplete restoration of salt diapirs and piercement structures various locations. Yet, any backstripping naturally fails to balance missing rock record unless stratal gaps and hiati are filled. Integration of stratigraphic forward modelling (e.g. Granjeon, 2014; Grohmann et al., 2021) with backstripping might help closing some unconformable gaps in the sedimentary record.

Formatted: Indent: First line: 0 cm

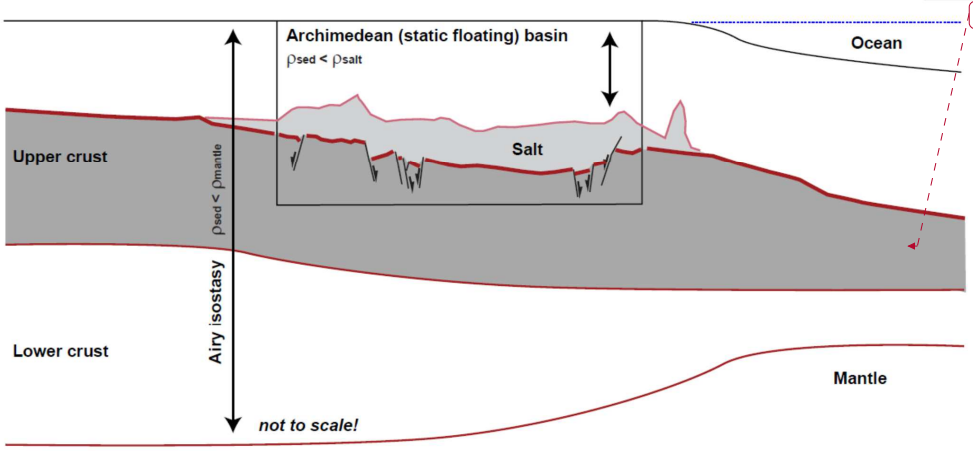

Formatted: Left

Figure 11. Scale and scope of the salt-restoration of this study in comparison to "classic" crustal-scale backstripping (e.g. Turcotte and Schubert, 2014). The concept of isostatic correction is essentially the same for calculating the total mass above a reference datum i) at great depth below the base of the crust; or ii) at Top salt, ignoring everything that happens below that level. Note that volumetrics, lateral distribution, thickness, state of aggregation and physical properties of the respective reconstruction base (salt/evaporites versus the Earth's mantle) are yet fundamentally different.

The salt reconstruction presented has furthermore omitted the restoration of any subsalt post-Zechstein deformation. Yet, if type, timing and magnitude of subsalt faulting or folding can be determined, 3D fault reconstruction or unfolding can be readily integrated into the restoration methodology proposed, in this case after unloading and prior to true-to-volume base Zechstein adjustment.

The magnitude of potential loss or influx of salt at the edges of the study area was finally estimated by comparing a first-pass scenario 1 restoration solely based on 3D block Groningen (Fig. 2) with the scenario 1 restoration of the entire NE Netherlands (Fig. 4~~a~~6a). This comparison showed before 200 Ma a mismatch between the regional and local scenario 1 reconstructions in the Groningen area of <10%. At 200 Ma, the large-scale restoration trailed the local Groningen balance by 0,14 x 10^{12} m^3 (ca. 12% of block volume). At 251 Ma, the large-scale reconstruction showed a lack of Zechstein by 0,47 x 10^{12} m^3 (ca. 40% of block volume) in the Groningen block in comparison to the local model. This imbalance between local and regional reconstructions indicates that true-to-volume balancing highly depends on model size and the amount of differential unloading. Highest precision true-to-volume balancing by unloading will be achieved in restorations that cover subsurface salt systems in full 3D extent; and in these systems in the youngest backstripping intervals.

The case study presented here for the onshore NE Netherlands concentrates on a structurally relatively simple area dominated by vertical subsidence, with little influence from thick-skinned tectonic activity. The applied method ~~therefore~~ yields in this area promising results. This may not work as successfully in other, more complex salt-tectonic provinces. For

example, if applied to areas where allochthonous salt sheets flow at the surface (e.g. Gulf of Mexico: e.g. Fletcher et al., 1996; Fort and Brun, 2012; Duffy et al., 2019); where complex structures such as salt canopies occur (e.g. Santos Basin: Jackson et al., 2015; Moroccan margin: Neumaier et al., 2016); or where large salt nappes have flowed many 10's of kilometres seaward, accommodating long-distance lateral translation of the overburden relative to the base-salt (e.g. offshore Angola; Fort et al., 2004; Hudec and Jackson, 2004), the simple Archimedean method applied here may prove insufficient. In such cases a reconstruction coupling 3D salt-thickness restoration and 3D tectonic retro-deformation might be successful.

6 Conclusions

1. 3D backstripping based on the ancient Archimedes' principle restored through time variations in 3D subsurface evaporite thickness; 3D salt loss and gain; 3D subsurface salt movement; and long-term salt-flow rates.

2. Sequential unloading of a solid sedimentary overburden floating on a pseudo-fluid evaporite substratum showed that subsurface evaporite movement reacts to any process that influences overburden thickness, in this case sedimentation, erosion and tectonics.

3. Limits of buoyancy-based 3D salt reconstruction include incomplete restoration due to overburden unconformities; uncertainty of the volumetric model integrity because of potential salt loss by dissolution; exclusion of subsalt deformation from restoration; and potential loss or influx of salt at the edges of the model area.

4. 3D subsurface salt restoration based on Archimedes' principle is mathematically simple and computationally quick. The approach presented can be potentially integrated into existing backstripping workflows. It can furthermore serve as a benchmark for physics-based numerical modelling of salt tectonics.

Data availability. Access to all seismic-reflection, borehole and geological surface data at www.nlog.nl (Dutch Oil and Gas portal). Lithology data from DINOLoket public database.

Author contributions. SB and SA performed data analysis. SB and SA interpreted the data under discussion with VS and RL. SB, SA, VS and RL wrote the final manuscript.

Acknowledgements. We thank the Netherlands Organisation for Applied Scientific Research (TNO) and the Nederlandse Aardolie Maatschappij (NAM) for seismic, borehole and horizon data; Schlumberger for Petrel software; and Petroleum Experts (Petex) for MOVE software. We acknowledge 4 anonymous reviews on an earlier version of this manuscript. Solid Earth reviewer Frank Peel is explicitly acknowledged for his very thorough, constructive and helpful review. Figures 4, 5, 10 and 11 of this paper were drawn following Frank's clear sketches and detailed suggestions. SA was funded by German Research Foundation (DFG) grant 403093957.

~~We acknowledge 3 anonymous reviews on an earlier version of this manuscript. SA is funded by German Research Foundation (DFG) grant 403093957.~~

Formatted: English (United States)

References

Aarhenius, S., and Lachmann, R.: Die physikalisch-chemischen Bedingungen der Bildung der Salzlagerstätten und ihre Anwendung auf geologische Probleme, Geologische Rundschau, 3, 139-157, 1912.

Airy, G.B.: On the Computations of the Effect of the Attraction of the Mountain Masses as Disturbing the Apparent Astronomical Latitude of Stations in Geodetic Surveys, Transactions of the Royal Society of London, 145, p. 101-104, 1855.

Alsop, G.I., Weinberger, R., Levi, T., and Marco, S.: Cycles of passive versus active diapirism recorded along an exposed salt wall, Journal of Structural Geology, 84, p. 47-67, 2016.

Archimedes: On floating bodies, in: The Works of Archimedes - Edited in Modern Notation with Introductory Chapters, edited by: Heath, T.L., Cambridge Library Collection - Mathematics, p. 253-262, 246 BC/2009.

Barton, D.C.: Mechanics of formation of salt domes with special reference to Gulf coast salt domes of Texas and Louisiana. AAPG Bulletin, 17, p. 1025–1083, 1933.

Biehl, B., Reuning, L., Strozyk, F., and Kukla, P.: Origin and deformation of intra-salt sulphate layers: an example from the Dutch Zechstein (Late Permian), International Journal of Earth Sciences, 103, p. 697-712, 2014.

Cartwright, J., Steward, S., and Clark, J.: Salt dissolution and salt-related deformation of the Forth Approaches Basin, UK North Sea, Marine and Petroleum Geology, 18, p. 757-778, 2001.

Casas, E., and Lowenstein, T. K.: Diagenesis of saline pan halite; comparison of petrographic features of modern, Quaternary and Permian halites, Journal of Sedimentary Petrology, 59, p. 724–739, 1989.

Davison, I.: Faulting and fluid flow through salt, Journal of the Geological Society, London, 166, p. 205–216, 2009.

Davison, I., Alsop, G. I., and Blundell, D. J.: Salt tectonics: some aspects of deformation mechanics, in: Salt Tectonics, edited by: Alsop, G. I., Blundell, D. J., and Davison, I., Geological Society, London, Special Publication 100, p. 1–10, 1996.

Duin, E.J.T, Doornenbal, J.C., Rijkers, R.H.B., Verbeek, J.W., and Wong, T.: Subsurface structure of the Netherlands: Results of recent onshore and offshore mapping, Netherlands Journal of Geosciences - Geologie en Mijnbouw, 85, p. 245 – 276, 2006.

Duffy, O.B., Fernandez, N., Peel, F.J., Hudec, M., Dooley, T.P., and Jackson, C.A.-L.: Obstructed Minibasins on a Salt-Detached Slope: An Example from above the Sigsbee Canopy, Northern Gulf of Mexico, Basin Research, 32, p. 505-524.

Fletcher, R.C., Hudec, M., and Watson, I.A.: Salt glacier and composite sediment-salt glacier models for the emplacement and early burial of allochthonous salt sheets, in: Salt tectonics: a global perspective, edited by: Jackson, M.P.A., Roberts, D.G., and Snelson, S., American Association of Petroleum Geologists Memoir 65, p. 77-108, 1996.

Formatted: English (United Kingdom)

Fort, X., Brun, J.-P., and Chauvel, F.: Salt tectonics on the Angolan margin, synsedimentary deformation processes, American Association of Petroleum Geologists Bulletin, 88, p. 1523–1544, 2004.

Fort, X., and Brun, J.-P.: Kinematics of regional salt flow in the northern Gulf of Mexico, in: Salt Tectonics, Sediments and Prospectivity, edited by: Alsop, G.I., Archer, S.G., Hartley, A. J., Grant, N.T., and Hodgkinson, R., Geological Society of London, Special Publication 363, p. 265-287, 2012.

Geluk, M.C.: Permian, in: Wong, T.E., Batjes, D.A.J., and De Jager, J., eds., Geology of the Netherlands, Royal Netherlands Academy of Arts and Sciences, Amsterdam, p. 63-84, 2007.

Gemmer, L., Ings, S.J., Medvedev, S., and Beaumont, C.: Salt tectonics driven by differential sediment loading: stability analysis and finite element experiments, Basin Research, 16, p. 199–218, 2004.

Giles, K.A., and Rowan, M.G.: Concepts in halokinetic-sequence deformation and stratigraphy, in: Salt Tectonics, Sediments and Prospectivity, edited by: Alsop, G.I., Archer, S.G., Hartley, A. J., Grant, N.T., and Hodgkinson, R., Geological Society of London, Special Publication 363, p. 7-31, 2012.

Granjeon, D.: 3D forward modelling of the impact of sediment transport and base level cycles on continental margins and incised valleys, in: From Depositional Systems to Sedimentary Successions on the Norwegian Continental Margin, edited by: Martinius, A.W., Ravnås, R., Howell, J. A., Steel, R. J., and Wonham, J. P., International Association of Sedimentologists Special Publication 46, p. 453-472, 2014.

Grohmann, S., Fietz, W.S., Nader, F.H., Romero-Sarmiento, M.-F., Baudin, F., and Littke, R.: Characterization of Late Cretaceous to Miocene source rocks in the Eastern Mediterranean Sea: An integrated numerical approach of stratigraphic forward modelling and petroleum system, Basin Research, 33, p. 846-874, 2021

Hudec, M., and Jackson, M.P.A.: Regional restoration across the Kwanza Basin, Angola: Salt tectonics triggered by repeated uplift of a metastable passive margin, American Association of Petroleum Geologists Bulletin, 88, p. 071-990, 2004.

Hudec, M., and Jackson, M.P.A.: Terra Infirma: understanding Salt Tectonics, Earth-Science Reviews, 82, p. 1-28, 2007.

Hunfeld, L.B., Foeken, J.P.T., and van Kempen, B.M.M.: Geomechanical parameters derived from compressional and shear sonic logs for main geothermal targets in The Netherlands. TNO: https://www.nlog.nl/sites/default/files/2021-12/data_selection_and_methods.pdf, last access: 11.04.2022.

Jackson, C.A.L., Jackson, M.P.A., Hudec, M.R., and Rodriguez, C.R.: Enigmatic structures within salt walls of the Santos Basin - Part 1: Geometry and kinematics from 3D seismic reflection and well data, Journal of Structural Geology, 75, p. 135-162, 2015.

Jackson, M.P.A., and Hudec, M.: Salt Tectonics: Principles and Practice, Cambridge University Press, 498 p., 2017.

Jackson, M.P.A., and Vendeville, B.C.: Regional extension as a geologic trigger for diapirism, Geological Society of America Bulletin, 106, p. 57-73, 1994.

Kehle, R.O.: Identifying suitable "piercement" salt domes for nuclear waste storage sites, Report PNL-2864 UC-70 prepared for the Office of Nuclear Waste Isolation under its Contract with the U.S. Department of Energy, Batelle Memorial Institute, p. 1-30, 1980.

Kehle, R.O.: The origin of salt structures, in B.C. Schreiber, ed., Evaporites and Hydrocarbons, Columbia University Press, New York, p. 345-404, 1988.

Khalifa, N., and Back, S.: Folding and faulting offshore Libya: Partly decoupled tectonics above evaporites, Marine and Petroleum Geology, 124, 104840, 2021.

Kley, J., and Voigt, T.: Late Cretaceous intraplate thrusting in central Europe: Effect of Africa-Iberia-Europe convergence, not Alpine collision, Geology, 36, p. 839-842, 2008.

Koyi, H.A.: Modeling the influence of sinking anhydrite blocks on salt diapirs targeted for hazardous waste disposal, Geology, 29, p. 387-390, 2001.

Kukla, P.A., Urai, J.L., and Mohr, M.: Dynamics of salt structures, in: Dynamics of complex intracontinental basins: The Central European Basin System, edited by Littke, R., Bayer, U., Gajewski, D., and Nelskamp, S., Berlin, Springer-Verlag, p. 291-306, 2008.

Maystrenko, Y.P., Bayer, U., and Scheck-Wenderoth, M.: Salt as a 3D element in structural modelling – Example from the Central European Basin System, Tectonophysics, 591, 62-82, 2013.

Mohr, M., Kukla, P.A., Urai, J.L., and Bresser, G.: Multiphase salt tectonic evolution in NW Germany: seismic interpretation and retrodeformation, International Journal of Earth Sciences, 94, p. 917-941, 2005.

Morley, C.K., and Guerin, G.: Comparison of gravity-driven deformation styles and behaviour associated with mobile shales and salt, Tectonics, 15, p. 1154-1170, 1996.

Nettleton, L.L.: Recent experiments and geophysical evidence of mechanics of salt dome formation, AAPG Bulletin, 27, p. 51-63, 1934.

Neumaier, M., Back, S., Littke, R., Kukla, P.A., Schnabel, M., and Reichert, C.: Late Cretaceous to Cenozoic geodynamic evolution of the Atlantic margin offshore Essaouira (Morocco), Basin Research, 28, p. 712-730, 2016.

Richter-Bernburg, G.: Salt Tectonics, Interior Structures of Salt Bodies, Bulletin Centres Recherches Exploration-Production Elf Aquitaine, 4, p. 373-389, 1980.

Rowan, M.G.: A systematic technique for the sequential restoration of salt structures, Tectonophysics, 228, p. 331-348, 2003.

Sclater, J.G., and Christie, P.A.F.: Continental stretching: An explanation of the Post-Mid-Cretaceous subsidence of the central North Sea Basin, Journal of Geophysical Research, 85, p. 3711-3739, 1980.

Strozyk, F., van Gent, H.W., Urai, J.L., and Kukla, P.A.: 3D seismic study of complex intra-salt deformation: An example from the Upper Permian Zechstein 3 stringer, western Dutch offshore, in: Salt Tectonics, Sediments and Prospectivity,

edited by: Alsop, G.I., Archer, S.G., Hartley, A.J., Grant, N.T., and Hodgkinson, R., Geological Society, London, Special Publication 363, p. 489-501, 2012.

Strozyk, F., Urai, J.L., van Gent, H.W., de Keijzer, M., and Kukla, P.A.: Regional variations in the structure of the Permian Zechstein 3 intrasalt stringer in the northern Netherlands: 3D seismic interpretation and implications for salt tectonic evolution, Interpretation, 2, p. SM101-SM117, 2014.

Ten Veen, J.H., van Gessel, S.F., and den Dulk, M.: Thin- and thick-skinned salt tectonics in the Netherlands; a quantitative approach, Netherlands Journal of Geosciences - Geologie en Mijnbouw, 91, p. 447-464, 2012.

TNO-NITG: Geological Atlas of the Subsurface of the Netherlands – onshore, Netherlands Organisation for Applied Scientific Research, 103 p., 2004.

TNO-NLOG: DGM-deep V5 regional subsurface layer model of The Netherlands. TNO: https://www.nlog.nl/en/details-dgm-deep-v5, last access: 08.05.2022.

Trusheim, F.: Über Halokinese und ihre Bedeutung für die strukturelle Entwicklung Norddeutschlands, Zeitschrift der deutschen geologischen Gesellschaft (ZDGG), 109, p. 111–151, 1957.

Trusheim, F.: Mechanism of salt migration in northern Germany, AAPG Bulletin, 44, p. 1519–1540, 1960.

Turcotte, D., and Schubert, G.: Geodynamics, Cambridge University Press, 636 p., 2014

Vackiner, A.A., Antrett, P. Strozyk, F., Back, S., Kukla, P.A., and Stollhofen, H.: Salt kinematics and regional tectonics across a Permian gas field: a case study from East Frisia, NW Germany, International Journal of Earth Sciences, 102, p. 1701-1716, 2013.

Van Adrichem Boogaert, H.A. & Kouwe, W.F.P.: Stratigraphic nomenclature of the Netherlands, revision and update by RGD and NOGEPA, Section A, General, Mededelingen Rijks Geologische Dienst 50: 1-40, 1993.

Van Dalfsen, W., Doornenbal, J.C., Dortland, S., and Gunnink, J.: A comprehensive seismic velocity model for the Netherlands based on lithostratigraphic layers, Netherlands Journal of Geosciences - Geologie en Mijnbouw, 85, p. 277 – 292, 2006.

van Keken, P.E., Spiers, C.J., van den Berg, A.P., and Muyzent, E.J.: The effective viscosity of rocksalt: implementation of steady-state creep laws in numerical models of salt diapirism, Tectonophysics, 225, p. 457–476, 1993.

Waltham, D.: Why does salt start to move?, Tectonophysics, 282, p. 117-128, 1997.

Warren, J.K.: Evaporites, Springer International Publishing, 1813 p., 2016.

Wong, T.E., Batjes, D.A.J., and de Jager, J. (Eds.): Geology of the Netherlands, Amsterdam, Royal Netherlands Academy of Arts and Sciences (KNAW), 354 p., 2007.

Zirngast, M.: The development of the Gorleben salt dome (northwest Germany) based on quantitative analysis of peripheral sinks, in: Salt Tectonics, edited by: Alsop, G.I., Blundell, D.J., and Davison, I., Geological Society, London, Special Publication 100, p. 203-226, 1996.

Formatted: Default Paragraph Font